# Skyrmion dynamics under uniaxial anisotropy

**Dieter Ehlers, I. Stasinopoulos, Vladimir Tsurkan, Hans-Albrecht Krug von Nidda, T. Fehér, A. Leonov, István Kézsmárki, D. Grundler, Alois Loidl**

**Angaben zur Veröffentlichung / Publication details:**

Ehlers, Dieter, I. Stasinopoulos, Vladimir Tsurkan, Hans-Albrecht Krug von Nidda, T. Fehér, A. Leonov, István Kézsmárki, D. Grundler, and Alois Loidl. 2016. "Skyrmion dynamics under uniaxial anisotropy." *Physical Review B* 94 (1): 014406. https://doi.org/10.1103/physrevb.94.014406.



# Skyrmion dynamics under uniaxial anisotropy

D. Ehlers,[1] I. Stasinopoulos,[2] V. Tsurkan,[1,3] H.-A. Krug von Nidda,[1] T. Fehér,[4] A. Leonov,[5] I. Kézsmárki,[4] D. Grundler,[2,6] and A. Loidl[1]

[1]*Experimentalphysik V, Elektronische Korrelationen und Magnetismus, Universität Augsburg, 86135 Augsburg, Germany*

[2]*Lehrstuhl für Physik funktionaler Schichtsysteme, Technische Universität München, Physik Department, 85748 München, Germany*

[3]*Institute of Applied Physics, Academy of Sciences of Moldova, MD 2028 Chisinau, Republica Moldova*

[4]*Department of Physics, Budapest University of Technology and Economics and MTA-BME Lendület Magneto-optical Spectroscopy Research Group, 1111 Budapest, Hungary*

[5]*IFW Dresden, Postfach 270016, 01171 Dresden, Germany*

[6]*EPFL STI IMX LMGN, MXC 241, Station 12, 1015 Lausanne, Switzerland*

(Received 9 December 2015; revised manuscript received 18 May 2016; published 6 July 2016)

Broadband microwave spectroscopy has been performed on single-crystalline $GaV_4S_8$, which exhibits a complex magnetic phase diagram including cycloidal and Néel-type skyrmion lattice phases below 13 K. At small magnetic fields two collective modes with large frequency separation are found that reflect the cycloid state subject to a large uniaxial anisotropy. In the skyrmion lattice phase three modes are resolved. Analyzing the spin-precessional motion microscopically, we explain the low frequency of the breathing mode in these Néel skyrmions by the hard-axis orientation of relevant spins.

DOI: 10.1103/PhysRevB.94.014406

## I. INTRODUCTION

The occurrence of spin patterns with nontrivial topologies has gained considerable interest in condensed matter physics. Recent research focuses on magnetic skyrmions which are thermodynamically stabilized whirl-like objects emerging in compounds with noncentrosymmetric crystal structures, in a limited region of the magnetic field versus temperature phase diagram [1–3]. They can crystallize in skyrmion lattices (SkLs) with typical lattice constants from 10 to 100 nm and give rise to emergent electrodynamics, like the topological Hall effect [4–6] or magnetic monopoles [7]. Individual skyrmions have been proposed as building blocks for future memory devices [8,9]. The SkL has also raised interest for microwave-technology applications after collective spin excitations predicted in the GHz range [10] were evidenced in the insulating chiral magnet $Cu_2OSeO_3$ [11–15]. Recently it was found that Bloch-type SkL states in various metallic, semiconducting, and insulating chiral magnets support three low-energy collective spin excitations characterized as clockwise (CW), counterclockwise (CCW), and breathing (BR) modes, which all follow a universal behavior [16].

Besides the Bloch-type skyrmions reported in the aforementioned works, a Néel-type SkL so far unobserved in bulk materials has recently been discovered in $GaV_4S_8$ [17–19], where the spins rotate radially towards the vortex core. In this semiconductor characterized by $V_4S_4$ molecular clusters with spin $S = \frac{1}{2}$ [20], a structural Jahn-Teller transition [21] at 44 K is followed by the onset of magnetic order at the Curie temperature $T_C = 13$ K. At the structural transition the lattice is stretched along one of the four body diagonals. The four distortion directions correspond to the magnetic easy axes of the four structural domains coexisting below 44 K. The magnetic state in each domain depends on the strength and orientation of the magnetic field with respect to the corresponding easy axis and gives rise to complex magnetic phase diagrams including cycloidal (Cyc), SkL, and ferromagnetic (FM) regions. The phases have been interpreted in terms of a competition of symmetric and of antisymmetric (Dzyaloshinskii-Moria, DM) exchange interactions, as well as of the Zeeman interaction. The phase diagrams, shown in Figs. 1(a)–1(c), have been derived from detailed magnetization measurements [17]. Roman superscripts distinguish equivalent magnetic phases realized in different domains over different field ranges. Unlike Bloch-type skyrmions, Néel-type skyrmions in $GaV_4S_8$ do not follow the external magnetic field but are confined to the magnetic easy axes [17]. Most interestingly it has been found that $GaV_4S_8$ is a multiferroic compound with orbitally derived ferroelectricity below the Jahn-Teller transition [19] and spin-driven excess polarizations in all magnetic phases, including magnetic skyrmions dressed with ferroelectric polarization [18].

In this article, we study the spin excitations in single-crystalline $GaV_4S_8$ by means of broadband microwave spectroscopy and work out the characteristic dynamics of the Néel-type skyrmion lattice. Performing such electron spin resonance experiments with the magnetic field applied along the principal cubic axes ⟨100⟩, ⟨110⟩, and ⟨111⟩, we find a series of characteristic resonances in all three magnetic phases, with substantial deviations from modes reported for compounds hosting Bloch-type skyrmions. We present a qualitative explanation for the hierarchy of skyrmion modes that underlines the importance of magnetic anisotropy for the skyrmion dynamics.

## II. EXPERIMENTAL DETAILS

$GaV_4S_8$ single crystals were prepared as described in Ref. [18]. Magnetic microwave spectroscopy was performed by inductive coupling of the sample to microwave fields of variable frequency $\nu$ between 10 MHz and 26.5 GHz above a coplanar waveguide (CPW) [16]. The external static magnetic field $H_{ext} = B/\mu_0$ (where $B$ denotes the magentic flux density and $\mu_0$ the vacuum permeability) was applied perpendicular to the CPW plane. As the signal line of the CPW was 20 $\mu$m wide, and thus much smaller than the diameter of the platelike

 

samples of about 1 mm, the setup provides both parallel and perpendicular components of the microwave field with respect to the static field. A network analyzer recorded the transmission of the microwave through the coplanar waveguide in terms of the amplitude of the scattering parameter $|S_{12}|$. To eliminate field-independent spectral features, the power transmission spectra recorded in the saturated FM state at $B = 2\,\mathrm{T}$ were subtracted, yielding the difference transmission spectra $\Delta|S_{12}(\nu)|$ shown here.

## III. RESULTS AND ANALYSIS

Figures 1(d)–1(f) compare typical difference transmission spectra obtained at 11 K for $B$ applied along the directions $\langle 100\rangle$, $\langle 110\rangle$, and $\langle 111\rangle$. At zero field in the cycloidal phase, we observe two well-separated absorptions, close to 5 and 15 GHz. For a quantitative analysis the zero-field spectra are

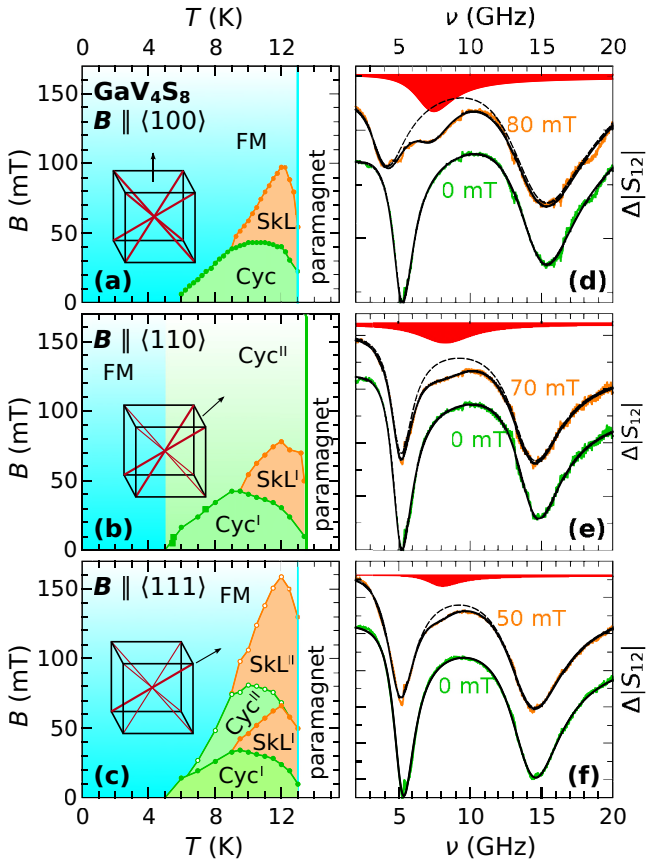


FIG. 1. (a)–(c) Magnetic phase diagrams of $GaV_4S_8$ for field directions (a) $B \parallel \langle 100\rangle$, (b) $B \parallel \langle 110\rangle$, and (c) $B \parallel \langle 111\rangle$, respectively. Cycloidal (Cyc, $Cyc^{I}$, $Cyc^{II}$) and skyrmion-lattice spin structures (SkL, $SkL^{I}$, $SkL^{II}$) are embedded in a ferromagnetic (FM) phase. Cubes and arrows illustrate the orientation of the external field with respect to the possible directions of the rhombohedral distortion, i.e., the body diagonals of the cube. (d)–(f) Selected difference transmission spectra at $T = 11\,\mathrm{K}$, for zero and finite fields in the respective field directions. The zero-field data are described by two Dysonian lines (solid lines), while the results at finite fields have been fitted with three Dysonians (solid lines). For the latter, the decomposition into outer lines (dashed lines) and the additional excitation in the SkL phase (solid pattern in red) is shown.

reasonably described by two Dysonian-shaped lines [22],

$$D(\nu) = \frac{I[\Delta\nu + \alpha(\nu - \nu_0)]}{(\nu - \nu_0)^2 + \Delta\nu^2},$$

superimposed on a weak linear background. Here $I$ is proportional to the integrated intensity, $\nu_0$ is the resonance frequency, $\Delta\nu$ is the linewidth, and $\alpha$ is the dispersion to absorption ratio [23]. As the sample is insulating, $\alpha$ originates from phase shifts due to impedance mismatches and not from conductivity contributions.

We now discuss the spectra obtained at finite field of a few 10 mT in the skyrmion-lattice phase, where the spectrum is well described by three Dysonian lines. First we focus on the case $B \parallel \langle 100\rangle$, where $B$ encloses the same angle of 55° with the easy axes of all the four possible domains, i.e., the $\langle 111\rangle$ directions. Consequently, the magnetic phase diagrams of all domains in Fig. 1(a) coincide and the observed spectra result from a unique phase. At 80 mT, in the SkL phase [Fig. 1(d)], the high-frequency (hf) mode resides near 15 GHz but is slightly broader compared to $B = 0\,\mathrm{T}$, while the low-frequency (lf) mode is shifted to 4 GHz. At the same time, a shoulder is observed indicating an additional resonance at 7.5 GHz characteristic of the SkL phase. To clearly illustrate this intermediate mode, we decompose the three-line fit into the two outer modes (dashed line) and the central line (solid pattern, highlighted in red color). In Figs. 1(b) and 1(e), where $B \parallel \langle 110\rangle$, two domains have their easy axes perpendicular to $B$ while the easy axes of the other two domains span an angle of 35° with $B$. In this case, the pronounced low- and high-frequency resonances remain close to 5 and 15 GHz at 70 mT, respectively. We again resolve the shoulder indicative for the $SkL^{I}$ phase, now at 8.5 GHz, but with only about half of the intensity as compared to $B \parallel \langle 100\rangle$, since the $SkL^{I}$ state develops only in two domains, while the other two domains with easy axes perpendicular to $B$ reside in the cycloidal state. A more extreme situation occurs for $B \parallel \langle 111\rangle$ [see Figs. 1(c) and 1(f)], when the SkL state first emerges for the unique domain with the easy axis parallel to $B$. In the other three domains, whose easy axes span 71° with the field, the cycloidal order persists up to higher fields. At 50 mT, the shoulder attributed to the $SkL^{I}$ phase appears at a frequency of 8 GHz with about a quarter of the intensity as compared to $B \parallel \langle 100\rangle$, because here only one out of four domains contributes. Even in the case of Fig. 1(f), where the new mode is weakest, a fit with three Dysonian lines reduces the square sum $\chi^2$ of the fit by 19% compared to a two-line fit, which corroborates the significance of the extra line in the data analysis.

Figure 2 presents the detailed spectral evolution from the cycloidal via the skyrmion lattice into the ferromagnetic phase for $B \parallel \langle 100\rangle$, the simplest case in the multidomain state due to the equivalence of the four domains with respect to the external field. The regions of magnetic phases, in this plot represented as different colors of the spectra, are estimated by the field interval where a three-line fit is still possible (skyrmion phase, $70 \leqslant B \leqslant 150\,\mathrm{mT}$). Note that the corresponding phase boundaries are somewhat higher than those obtained from the magnetization measurements in Ref. [17]. We attribute this discrepancy to different demagnetization tensors in the samples used in this work. In the Cyc phase ($B \leqslant 60\,\mathrm{mT}$), the eigenfrequencies of the two lines are almost field independent.

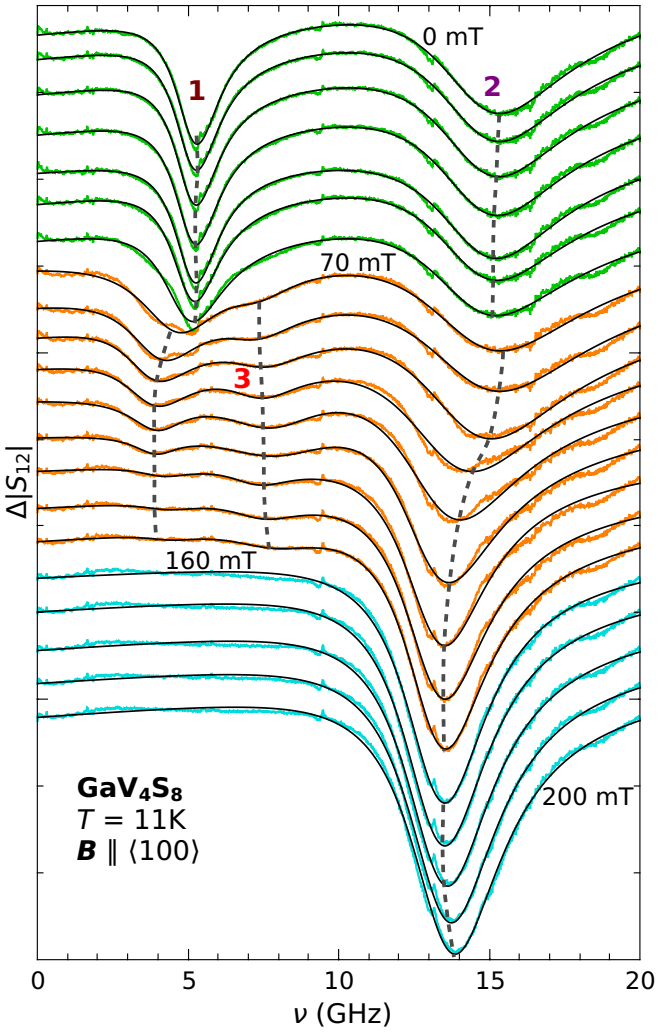


FIG. 2. Frequency dependence of microwave transmission in $GaV_4S_8$ at different external magnetic fields $0 \leqslant \mu_0 H_{\rm ext} \leqslant 200$ mT along ⟨100⟩. For clarity the spectra measured in steps of 10 mT are shifted vertically by a constant value. Green, orange, and cyan curves are spectra in the cycloidal, SkL, and ferromagnetic phases whereby black lines represent Dysonian fits using two, three, or one line, respectively (see text).

Concerning the resonance frequencies, the spectra together with their fit curves suggest that the boundary between SkL and Cyc phases is jumplike, whereas the transition into the ferromagnetic phase does not show any anomaly.

The fact that the skyrmion phase indeed exhibits three excitations is convincingly documented in Fig. 1. In order to clarify the field range where the SkL phase really requires three lines to describe the data, a look into the intensity evolution of the three fitted resonance lines together with confidence intervals in Fig. 3 provides elucidating information. The assignment of excitations to BR, CW, and CCW character as known for the three modes of Bloch-type SkLs will be justified in the discussion. In the Cyc phase the intensities of the two characteristic lines remain essentially constant, with the lower approximately half as intense as the upper. On passing into the SkL phase the intensity of the upper mode shows a steplike increase by approximately 20%. In contrast, the intensity of

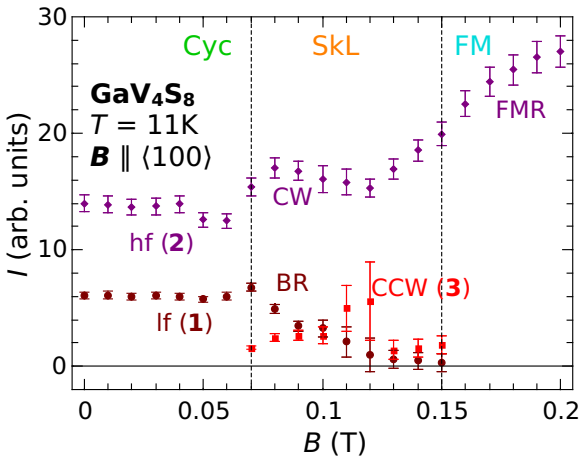


FIG. 3. Field dependence of the mode intensities obtained from Dysonian fits. Cyc phase: high-frequency (hf) and low-frequency (lf) modes; SkL phase: CW, CCW, and BR modes; polarized FM phase: ferromagnetic resonance (FMR). Dashed lines are drawn to guide the eye and the numberings 1, 2, and 3 refer to dashed lines in Fig. 2.

the lower mode decreases with increasing field and vanishes above 130 mT. The intensity of the additional intermediate line increases linearly with increasing field and abruptly diminishes at 130 mT. In the FM phase ($B > 150$ mT), only the upper mode remains, showing linearly increasing intensity with increasing field. Error bars in Fig. 3 have been estimated by the definition that the weaker lines become irrelevant (relative error 1), when the enhancement of $\chi^2$ due to their absence is equal to the $\chi^2$ enhancement due to a frequency deviation of the pronounced hf line by 5% of its linewidth, a deviation from the ideal fit which generally is sufficiently well visible by eye. This procedure takes into account the significance of the weaker lines and provides a more confident error analysis than by inspection of signal-to-noise ratios only. Additionally, for some spectra the influence of an uncertainty in $\alpha$ for the hf line needs to be accounted for. Now it becomes clear from Fig. 3 that the weaker lines with eigenfrequencies at 4 and 8 GHz remain significant at least up to 110 mT, which is lower than the phase boundary drawn in Figs. 2 and 3, but is still in good agreement with the expectation of a higher field value as compared to the phase diagram in Fig. 1(a).

The detailed field dependencies of the excitation spectra along the three principal cubic axes are summarized in the color-coded plots of Fig. 4. The symbols indicate resonance frequencies extracted from fitting Dysonian lines to the spectra. Error bars in this context are usually given by 10% of the linewidth, but here again they may also account for uncertainties in $\alpha$. In Figs. 4(a), 4(b), and 4(c), at 0 mT, we observe two excitations close to 5 and 15 GHz representative of the cycloidal phase of $GaV_4S_8$. Entering the SkL phases, three modes are observed. The different hierarchy of modes BR, CW, and CCW that we encounter is substantiated below. While the lower (BR) and upper (CW) branches soften, i.e., $d\nu_0/dB < 0$, the intermediate resonance (CCW) follows the opposite behavior with $d\nu_0/dB > 0$. These facts, softening of the BR and CW modes and hardening of the CCW mode, are also indicated in Fig. 2. The topmost branch always is the most prominent one. On passing the $SkL^1$ phase in Figs. 4(b) and 4(c)

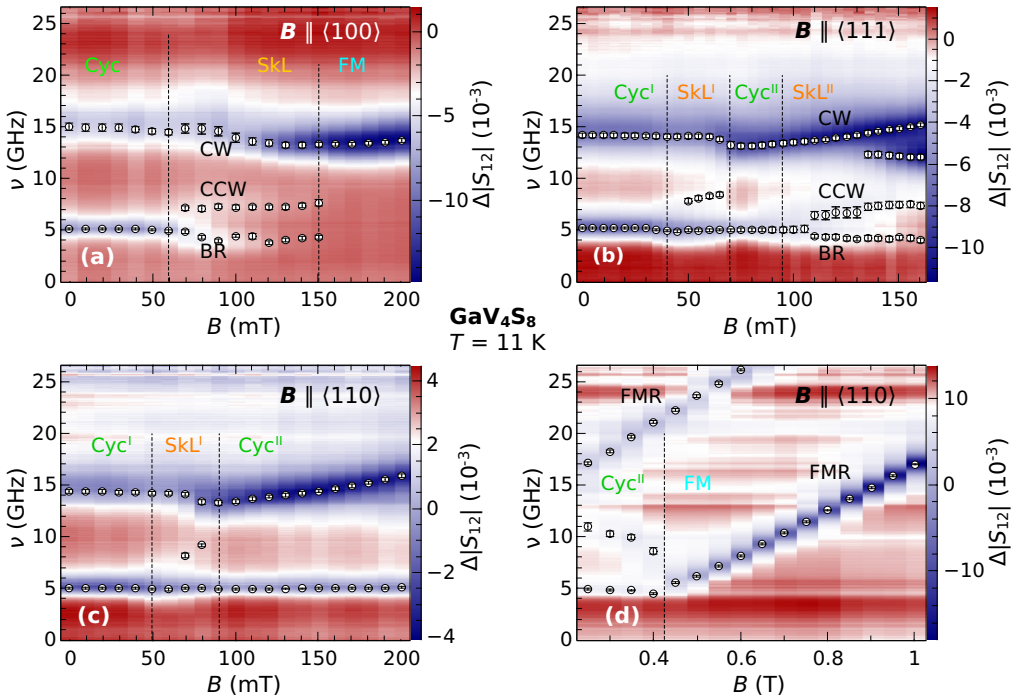


FIG. 4. (a)–(d) Color-coded plots of the transmission spectra $\Delta|S_{12}|$ in the frequency vs magnetic field plane for $T = 11$ K for the field applied along the cubic principal directions. The intermediate white color has been shifted in order to emphasize weak amplitudes. Open circles with error bars are resonance frequencies from the Dysonian fits (see text). Dashed lines indicate transitions between cycloidal (Cyc), skyrmion lattice (SkL), and ferromagnetic (FM) phases. Panels (a)–(c) display low-field regimes, whereas panel (d) shows the spin-flop behavior at higher fields.

we do not resolve a clear softening of the upper and lower modes due to the superimposed resonances from the domains that still exist in the cycloidal state at these fields. Differences in the slope of the intermediate modes of the SkL phases are attributed to different projections of the field onto the relevant easy axes of the domains contributing to the spin resonance. Beyond the SkL phases, the intermediate mode fades out, while the upper mode strengthens and changes to positive slope $d\nu_0/dB > 0$, as is typical for a ferromagnetic resonance (FMR). In the case of $B \parallel \langle 110\rangle$, where the easy axes of two domains are perpendicular to the field, the upper cycloidal mode of the $\mathrm{Cyc}^{\mathrm{II}}$ phase softens on increasing field and directly transforms into the FMR via a spin-flop transition near 0.45 T, where it meets with the field-independent lf mode, as evidenced in Fig. 4(d). A spin-flop behavior without softening to zero frequency is also described in Ref. [24], where the eigenfrequency of the spin helix has been calculated. The FMR mode at highest frequency, which increases continuously in this field range, stems from the two domains where parallel components of the external field with respect to their easy axes induce the ferromagnetic state already at 90 mT.

## IV. CONCLUDING DISCUSSION

We now compare our results on Néel skyrmions to the previously reported universal behavior in Bloch-type skyrmion hosts [16]. While in the Bloch-type systems in the helical phase at zero field the resonance modes lie close to each other, two well-separated modes exist in the cycloidal phase of the system under investigation. This strong zero-field splitting, also responsible for the field independence of the resonances for $B \lesssim 50$ mT, is attributed to the robust easy-axis magnetic anisotropy present in $GaV_4S_8$ but missing in cubic helimagnets. With the average isotropic exchange $J/k_B = 4.2$ K and the exchange anisotropy $\Delta J(2\,K)/k_B = 0.2$ K taken from Ref. [17], the antiferromagnetic gap can be estimated [25] as $\nu \sim (J\Delta J)^{1/2}/h = 19$ GHz at lowest temperatures, which is in good agreement with the observed frequency $\nu_0 = 15$ GHz of the upper mode at 11 K where the anisotropy is only 50% of the low-temperature value. Here $k_B$ and $h$ denote the Boltzmann constant and the Planck constant, respectively. Due to the DM pattern unique for polar magnets with $C_{nv}$ symmetry, the conical phase—being the main competitor of the SkL state in cubic helimagnets—does not emerge in $GaV_4S_8$ unless the magnetic field is (nearly) perpendicular to the easy axis, as it is realized for $B \parallel \langle 110\rangle$ in Figs. 4(c) and 4(d). In this extreme case the conical to FM transition is associated with a spin flop which is manifested in the softening of the hf mode, while the lf mode remains nearly field independent up to the spin flop. For other directions of the magnetic field, due to the suppression of the conical phase, the SkL state extends over a large region of the phase diagram. In such cases, shown in Figs. 4(a) and 4(b), no anomaly in the resonance frequencies is observed when approaching the SkL to FM transition with increasing fields. Instead, all three modes are smoothly transformed to the FMR at the transition. This is in strong contrast to spin dynamics in cubic helimagnets, where the FM state is always reached from the conical phase via a spin flop, which is driven by the softening of the excitation in the conical state.

In both, the Bloch- and Néel-type SkL phases, three eigenmodes are obtained, which are labeled CW, CCW, and

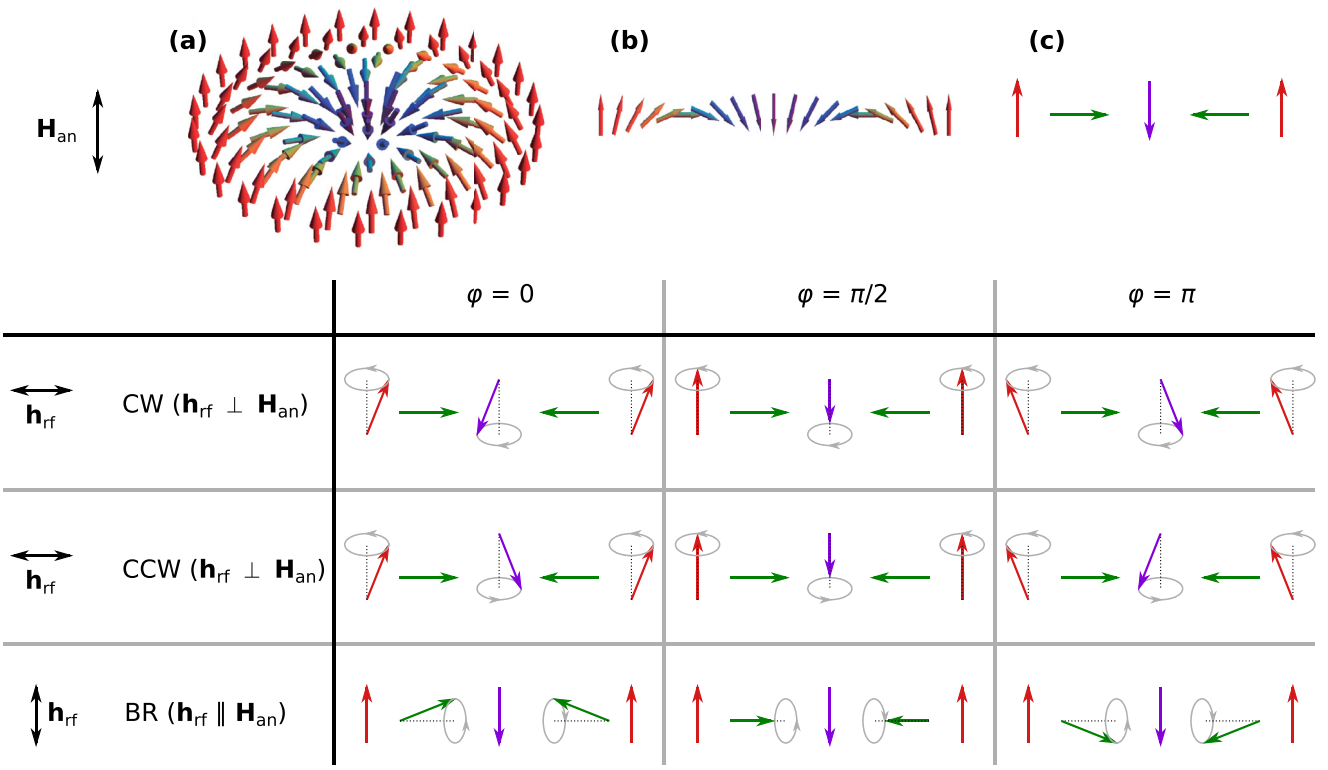


FIG. 5. Upper part: (a) Schematic illustration of a Néel-type skyrmion for a given easy axis of anisotropy $\mathbf{H}_{an}$. Each cross section (b) containing the skyrmion core corresponds to a spin cycloid and its simplification (c) to five spins comprises only vertical and horizontal arrows. Lower part: Table representing the spin dynamics of the five selected spins. The three rows stand for the three dynamic spin precessional modes (see text), whereas the three columns stand for three snapshots in time with corresponding phase $\varphi$. See the text for an explanation of the motion of the skyrmion core. The relation between the oscillating field $\mathbf{h}_{rf}$ and the anisotropy field $\mathbf{H}_{an}$ is different for CW and CCW modes as compared to the BR mode.

BR. Figure 5 shows a sketch of a Néel-type skyrmion, a cross section through the skyrmion core and its schematic simplification into five spins. This simplified spin pattern is used to illustrate single spin motions in the three cases and it is easily verified that they correspond to a clockwise and counterclockwise gyration as well as to a breathinglike expansion and contraction of the dynamic skyrmion core. In the CW case and at $\varphi = 0$ in Fig. 5, the dynamic core (spin pointing exactly downwards) is shifted somewhat to the left from the central, purple arrow, which represents the static skyrmion core. This is seen from the sense of rotation of spins within the simplified cycloid when moving to the left. A quarter period later, at $\varphi = \pi/2$, the dynamic skyrmion core is located behind the central spin and, consequently, the sense of gyration is clockwise. In the CCW case and at $\varphi = 0$ the dynamic core is shifted slightly to the right from the central arrow. A quarter period later, the dynamic skyrmion core is located behind the central spin again. Thus, the sense of gyration is counterclockwise. For the breathing mode, the core is shrunk at $\varphi = 0$, whereas it is enlarged at $\varphi = \pi$.

The CCW mode of Bloch-type skyrmions is known to exhibit a positive slope $d\nu_0/dB > 0$, while the BR mode shows a negative slope. The CW mode is rather field independent [16]. In $GaV_4S_8$ we find a significant positive slope always for the intermediate mode, while the mode with the lowest frequency exhibits a weak negative slope [see Figs. 4(a)–4(c)]. Hence, we assign the lowest mode as the BR mode. The low frequency of the BR mode can be understood microscopically by considering the bottom row of Fig. 5. This mode is excited by the oscillating field component $\mathbf{h}_{rf}$ parallel to the axis of the SkL core spins [12]. For the Néel-type SkL studied here, the relevant axis is defined by the uniaxial anisotropy field $\mathbf{H}_{an}$. Importantly, the torque provided by $\mathbf{h}_{rf}$ is nonzero and maximum for the spins being orthogonal to $\mathbf{H}_{an}$. For such spins the effective field entering the equation of motion is reduced as, in a hard-axis spin configuration, the anisotropy field counteracts the applied field [25]. Consequently, the eigenfrequency is low. This is a major difference compared to Bloch-type skyrmions, which explains the different sequence of branches. The dynamic spin components of the CW and CCW modes (two upper rows in Fig. 5), excited by the perpendicular component of the rf field, behave in analogy with optical and acoustic phonons, respectively. For the uppermost mode (CW, optical), dynamic components of the precessing spins periodically point against each other enhancing the restoring forces between them. For the CCW (acoustic) mode, dynamic spin components are parallel instead, consistent with smaller restoring forces and a smaller eigenfrequency compared to a CW motion. Still, its frequency is larger than that of the BR mode, because for the CCW case $\mathbf{H}_{an}$ adds to the applied field and enhances the effective field. Note at this point the opposite senses of precession for the central spin in Fig. 5. Like in conventional antiferromagnetic resonance, spins can perform either left-handed or right-handed precessions as

long as anisotropies are dominant over an external magnetic field.

In summary, we explore the spin dynamics in a Néel-type skyrmion lattice, realized in bulk $GaV_4S_8$. Starting from low magnetic fields, in the cycloidal phase, due to anisotropic exchange, two clearly separated resonance modes are observed. Three excitations evolve in the skyrmion lattice phase which, from lowest to highest frequency, can be ascribed to breathing, counterclockwise, and clockwise modes. In comparison to Bloch-type SkLs the internal anisotropy interchanges the hierarchy of excitations.

## ACKNOWLEDGMENTS

This work was supported by the Deutsche Forschungsgemeinschaft (DFG) via the Transregional Collaborative Research Center TRR 80: From Electronic Correlations to Functionality (Augsburg, Munich, Stuttgart) and by the Hungarian Scientific Research Fund OTKA (Grants No. K 107228 and No. K 108918). The authors wish to thank D. Vieweg for performing magnetometry measurements and S. Bordács for fruitful discussions. M. Mochizuki kindly provided us with a figure.

[1] A. Bogdanov and D. Yablonskiĭ, Sov. Phys. JETP **68**, 101 (1989).
[2] A. Bogdanov and A. Hubert, J. Magn. Magn. Mater. **138**, 255 (1994).
[3] A. Bogdanov and A. Hubert, Phys. Status Solidi B **186**, 527 (1994).
[4] A. Neubauer, C. Pfleiderer, B. Binz, A. Rosch, R. Ritz, P. G. Niklowitz, and P. Böni, Phys. Rev. Lett. **102**, 186602 (2009).
[5] N. Kanazawa, Y. Onose, T. Arima, D. Okuyama, K. Ohoyama, S. Wakimoto, K. Kakurai, S. Ishiwata, and Y. Tokura, Phys. Rev. Lett. **106**, 156603 (2011).
[6] R. Ritz, M. Halder, M. Wagner, C. Franz, A. Bauer, and C. Pfleiderer, Nature (London) **497**, 231 (2013).
[7] P. Milde, D. Köhler, J. Seidel, L. M. Eng, A. Bauer, A. Chacon, J. Kindervater, S. Mühlbauer, C. Pfleiderer, S. Buhrandt, C. Schütte, and A. Rosch, Science **340**, 1076 (2013).
[8] A. Fert, V. Cros, and J. Sampaio, Nat. Nanotechnol. **8**, 152 (2013).
[9] J. Sampaio, V. Cros, S. Rohart, A. Thiaville, and A. Fert, Nat. Nanotechnol. **8**, 839 (2013).
[10] M. Mochizuki, Phys. Rev. Lett. **108**, 017601 (2012).
[11] S. Seki, X. Z. Yu, S. Ishiwata, and Y. Tokura, Science **336**, 198 (2012).
[12] Y. Onose, Y. Okamura, S. Seki, S. Ishiwata, and Y. Tokura, Phys. Rev. Lett. **109**, 037603 (2012).
[13] Y. Okamura, F. Kagawa, M. Mochizuki, M. Kubota, S. Seki, S. Ishiwata, M. Kawasaki, Y. Onose, and Y. Tokura, Nat. Commun. **4**, 2391 (2013).
[14] Y. Okamura, F. Kagawa, S. Seki, M. Kubota, M. Kawasaki, and Y. Tokura, Phys. Rev. Lett. **114**, 197202 (2015).
[15] S. Zhang, J. Wang, Q. Zheng, Q. Zhu, X. Liu, S. Chen, C. Jin, Q. Liu, C. Jia, and D. Xue, New J. Phys. **17**, 023061 (2015).
[16] T. Schwarze, J. Waizner, M. Garst, A. Bauer, I. Stasinopoulos, H. Berger, C. Pfleiderer, and D. Grundler, Nat. Mater. **14**, 478 (2015).
[17] I. Kézsmárki, S. Bordács, P. Milde, E. Neuber, L. M. Eng, J. S. White, H. M. Rønnow, C. D. Dewhurst, M. Mochizuki, K. Yanai, H. Nakamura, D. Ehlers, V. Tsurkan, and A. Loidl, Nat. Mater. **14**, 1116 (2015).
[18] E. Ruff, S. Widmann, P. Lunkenheimer, V. Tsurkan, S. Bordács, I. Kézsmárki, and A. Loidl, Sci. Adv. **1**, e1500916 (2015).
[19] Z. Wang, E. Ruff, M. Schmidt, V. Tsurkan, I. Kézsmárki, P. Lunkenheimer, and A. Loidl, Phys. Rev. Lett. **115**, 207601 (2015).
[20] H. Nakamura, H. Chudo, and M. Shiga, J. Phys.: Condens. Matter **17**, 6015 (2005).
[21] R. Pocha, D. Johrendt, and R. Pöttgen, Chem. Mater. **12**, 2882 (2000).
[22] F. J. Dyson, Phys. Rev. **98**, 349 (1955).
[23] S. E. Barnes, Adv. Phys. **30**, 801 (1981).
[24] M. Kataoka, J. Phys. Soc. Jpn. **56**, 3635 (1987).
[25] A. G. Gurevich and G. A. Melkov, *Magnetization Oscillations and Waves* (CRC Press, Boca Raton, FL, 1996).